THE JOURNAL OF PHYSICAL CHEMISTRY B

Article

Cite This: J. Phys. Chem. B 2017, 121, 11210−11218

pubs.acs.org/JPCB

Structure of $ZnCl_2$ Melt. Part II: Fragile-to-Strong Transition in a Tetrahedral Liquid

Pierre Lucas,*[,†] Garrett J. Coleman,[†] Manga Venkateswara Rao,[†] Angharad N. Edwards,[†] Chrishani Devaadithya,[†] Shuai Wei,[†,‡,§] Abduljabar Q. Alsayoud,[†,∥] B. G. Potter, Jr.,[†] Krishna Muralidharan,[†] and Pierre A. Deymier[†]

[†]Department of Materials Science and Engineering, University of Arizona, Tucson, Arizona 85721, United States

[‡]School of Molecular Sciences, Arizona State University, Tempe, Arizona 85287, United States

ABSTRACT: The fraction of edge- and corner-sharing tetrahedra in liquid $ZnCl_2$ is quantified as a function of temperature using Raman spectroscopy and ab initio molecular dynamic simulations. Two distinct regimes are found in the temperature dependence of the change in these structural units. This behavior is consistent with the existence of a fragile-to-strong transition in liquid $ZnCl_2$ as suggested by calorimetric and viscosity measurements. The structural origin of this transition is rationalized in terms of a constraint counting formalism. It is suggested that the ratio of edge- to corner-sharing tetrahedra controls the configurational entropy and in turn the viscosity of the melt. The temperature dependence of this ratio above the melting point is also found to be qualitatively consistent with neutron diffraction data. The observation of a similar fragile-to-strong transition in the isostructural $GeSe_2$ melt indicates that it may be a common feature of tetrahedral liquids.

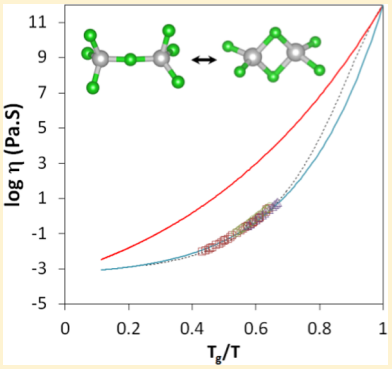

1. INTRODUCTION

Ionic melts based on $ZnCl_2$ have recently met renewed technological interest because of their potentials as heat-transfer fluids for concentrated solar power plants.[1−3] In that respect, viscosity is a critical property because these heat-transfer fluids must be pumped through an extensive network of pipes and heat exchangers. A deeper understanding of the factors that control the viscosity of $ZnCl_2$ melts is therefore of much technological importance.

On a fundamental level, $ZnCl_2$ is of interest because of its ability to bypass crystallization upon rapid cooling, thereby forming a supercooled liquid and eventually solidifying into a glass. Indeed, $ZnCl_2$ constitutes a rare prototype of ionic network glass and has been extensively investigated over the years both experimentally[4−14] and theoretically.[15−21] It is broadly accepted that the melt structure is composed of $ZnCl_4$ tetrahedral building blocks in a way similar to that in silica.[4−6,15−17] The liquid viscosity and its evolution with temperature are then determined by the way these building blocks interconnect. The transport properties of $ZnCl_2$ melts were first described using the "bond lattice" model of Angell and Rao,[21] where an increasing population of nonbridging chlorine atoms is created with increasing temperature. The probability of a mass transport event is then exponentially related to the fraction of broken bridges because of the increment in lattice entropy induced by each elementary excitation. The resulting viscosity−temperature dependence was shown to follow the conventional Vogel−Fulcher−Tammann form.[21] However, although broken chlorine bridges should undoubtedly contribute to a change in liquid dynamics, recent neutron diffraction[5] and Raman spectroscopy[6] studies on high-temperature melts suggest that the fraction of these broken bridges is minimal and would be too small to account for the large decrease in viscosity with temperature. Indeed, $ZnCl_2$ is considered to be an intermediate liquid on the Angell fragility scale[22] with a pronounced non-Arrhenius viscosity−temperature dependence.[11−14]

The objective of this work is therefore to reinvestigate the structural origin of dynamic flow in $ZnCl_2$ in view of recent spectroscopic observations that reveal the formation of increasing fractions of edge-sharing tetrahedra at high temperature.[5−7,23] Indeed, molecular dynamic simulations of MX_2 tetrahedral liquids have shown a strong correlation between melt fragility and the fraction of edge-sharing tetrahedra.[17] High-temperature Raman spectroscopy and ab initio molecular dynamics (AIMD) were therefore used to characterize the ratio of edge- to corner-sharing tetrahedra above the melting point as well as in the supercooled liquid. It was found that the temperature dependence of this ratio follows two distinct regimes, indicative of a fragile-to-strong transition. This behavior is consistent with calorimetric measurements revealing an unexpectedly strong behavior for $ZnCl_2$ near T_g, in contrast to the high fragility measured above the melting point. A similar behavior is observed in the isostructural $GeSe_2$ tetrahedral system.

Received: November 2, 2017
Revised: November 19, 2017
Published: November 22, 2017

DOI: 10.1021/acs.jpcb.7b10857
J. Phys. Chem. B 2017, 121, 11210−11218

2. METHODS

2.1. High-Temperature Raman Spectroscopy. Raman spectroscopy was performed on high-purity (99.999%) anhydrous $ZnCl_2$ samples (melting point T_m = 315 °C) stored at all times in a glove box under a high-purity argon atmosphere (<0.1 ppm H_2O and O_2). The Raman spectra were collected in the backscattering configuration through a microscope objective using an argon ion laser source (514 nm). As shown in Figure 1, the $ZnCl_2$ melt can be accessed in two different temperature regions; hence, the series of spectra were collected in two different temperature ranges: one above the melting point from 325 to 500 °C and the other in the supercooled liquid region from the glass-transition temperature, T_g = 112 °C, to the recrystallization temperature, T_x = 180 °C. For the high-temperature range, spectra were collected every 25 °C using a Jobin-Yvon Horiba Lab Ram HR800 spectrometer in an inverted microscope configuration and a custom-made heating stage consisting of a heating block fitted with four symmetrically positioned heating cartridges containing the $ZnCl_2$ sample within a flame-sealed silica vial. The cell temperature was equilibrated for 45 min before each spectrum collection. More details of this system are reported in ref 6. All Raman spectra were subjected to a linear baseline correction and thermally reduced to account for the temperature dependence of the scattering intensity.

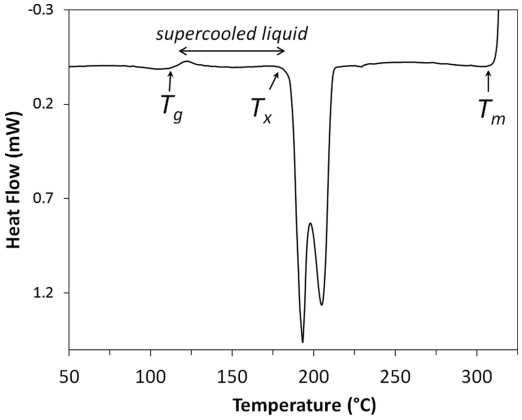

Figure 1. Differential scanning calorimetry (DSC) thermogram of amorphous $ZnCl_2$ quenched in water and scanned at a rate of 5 °C/min. The supercooled liquid region extends from T_g to T_x.

For the supercooled liquid range, it is not possible to equilibrate the temperature before recording each spectrum because of the strong driving force for crystallization; hence, a temperature scanning stage was used to collect the spectra continuously at a rate of 5 °C/min. At this rate, the supercooled liquid is stable from T_g to T_x, as shown in Figure 1. Spectra were collected every 5 °C with a collection time of 60 s using a 10× (NA = 0.28) microscope objective and a Renishaw InVia spectrometer with a 1200 lines/mm grating. The heating stage used for this measurement was a High-Temperature Reaction Chamber HVC-MRA-5 from Harrick Scientific. The stage was dried in an oven prior to each measurement, and the $ZnCl_2$ sample (a few milligram) was loaded in the sample cup inside the glove box and hermetically sealed in the chamber. The temperature of the sample cup was calibrated before the experiment using an individual thermocouple.

2.2. Differential Scanning Calorimetry. The stability range and the activation energy for enthalpy relaxation of amorphous $ZnCl_2$ were characterized using a differential scanning calorimeter DSC1 with an FRS5 sensor from Mettler Toledo. The sample and DSC pan preparations were performed in a glove box under an argon atmosphere. Approximately 5 mg of amorphous $ZnCl_2$ was loaded in a hermetic Tzero aluminum pan, from TA Instrument, and sealed hermetically. An identical empty pan was used as the reference.

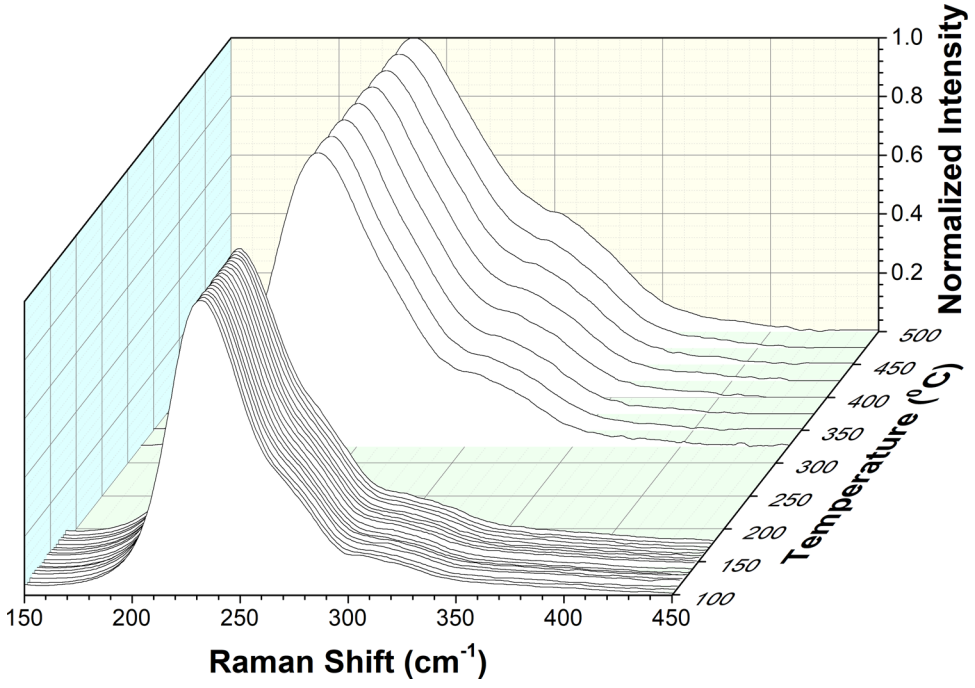

Figure 2. Normalized Raman spectra of liquid $ZnCl_2$ as a function of temperature. The spectra cover the supercooled liquid range as well as the stable liquid above T_m.

DOI: 10.1021/acs.jpcb.7b10857
J. Phys. Chem. B 2017, 121, 11210−11218

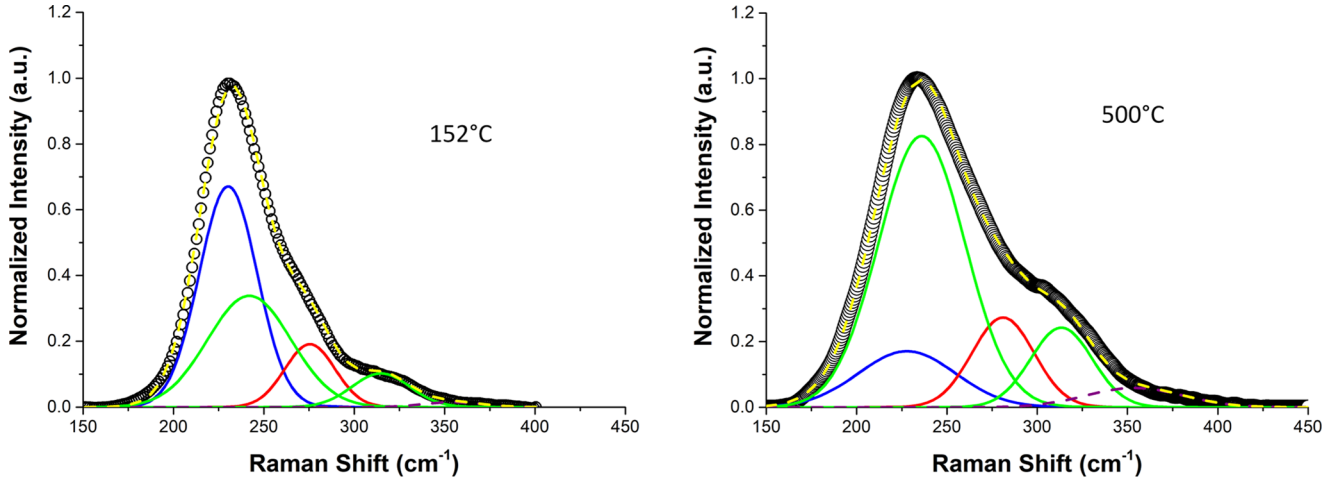

Figure 3. Peak-fitting of liquid $ZnCl_2$ Raman spectra at 152 and 500 °C. Peak assignment is detailed in the text and in ref 6.

The pans were then introduced in the calorimeter and scanned at fixed heating rates ranging from 3 to 30 K/min. For T_g determination as a function of the heating/cooling rate, the sample was first heated above T_g (but below T_x) and then cooled and reheated at the same rate. The T_g was defined as the onset of the heat capacity jump. Each measurement was repeated 2−3 times.

An identical procedure was used to characterize the activation energy for enthalpy relaxation of amorphous $GeSe_2$. The $GeSe_2$ sample was synthesized from high-purity (99.999%) elements, sealed in a 6 mm diameter silica tube under high vacuum (10^{-6} Torr). The melt was homogenized in a rocking furnace for 24 h at 900 °C prior to quenching in water into a glass rod. The glass homogeneity was confirmed by Raman and energy-dispersive spectroscopy.

2.3. Ab Initio Molecular Dynamic Simulations. AIMD simulations of $ZnCl_2$ melts were performed at 600, 800, and 900 K. Simulations were carried out with the Vienna Ab initio Simulation Package[24,25] using the projector augmented wave[26,27] method with the Perdew−Burke−Ernzerhof[28] exchange-correlation functional. Run times of 17.88 ps yielded convergence of the populations of various structural features such as corner- or edge-sharing tetrahedral units within ±1.1%. The structural analysis of $ZnCl_2$ liquids was performed using the R.I.N.G.S code.[29] Further details of modeling parameters are reported in ref 6.

3. RESULTS AND DISCUSSION

3.1. High-Temperature Raman Spectroscopy. Figure 2 shows the temperature-dependent Raman spectra of liquid $ZnCl_2$ from 100 to 500 °C. The gap in the data set corresponds to the region of crystallinity. All spectra were normalized for peak-fitting analysis using the intensity of the main peak near 225 cm^{-1}.

The main spectral feature is a notable increase in intensity of the side shoulder in the 300−350 cm^{-1} range with increasing temperature. This is particularly pronounced in the high-temperature region. Broadening of the main peak near 225 cm^{-1} is also apparent. However, a quantitative analysis of these spectral features requires a systematic peak-fitting analysis. Raman peak assignments for $ZnCl_2$ have been previously established using first-principles calculations.[6] It was shown that three distinct types of Zn local environments are present denoted $Zn^{(0)}$, $Zn^{(1)}$, and $Zn^{(2)}$ for a tetrahedron that shares all corners but no edge, shares one edge, and shares two edges with other tetrahedra, respectively.[23] It was found that these units generate four Raman modes centered at 225 cm^{-1} (peak 1), 274 cm^{-1} (peak 2), 237 cm^{-1} (peak 3), and 307 cm^{-1} (peak 4). Whereas the mode at 274 cm^{-1} corresponds to pure $Zn^{(2)}$, the remaining modes correspond to a combination of $Zn^{(1)}$ and $Zn^{(0)}$ as detailed in ref 6 according to

$$\%Zn^{(0)} = \%\text{peak } 1 + \%(0.5 \times \text{peak } 3 + 0.5 \times \text{peak } 4)$$

$$\%Zn^{(1)} = \%(0.5 \times \text{peak } 3 + 0.5 \times \text{peak } 4)$$

$$\%Zn^{(2)} = \%\text{peak } 2$$

It is then possible to perform curve-fitting to monitor the evolution of each structural unit with temperature. Examples of curve-fitting for a low- and a high-temperature spectrum are shown in Figure 3. A fifth peak corresponding to $ZnCl_3$ units with broken chlorine bridges is also necessary to optimize the fit, but these features remain lower than ∼5% of the total structure and are ignored in further analysis.

The results of curve-fitting analysis are summarized in Figure 4. It is clear that the population of $Zn^{(0)}$ decreases, whereas the

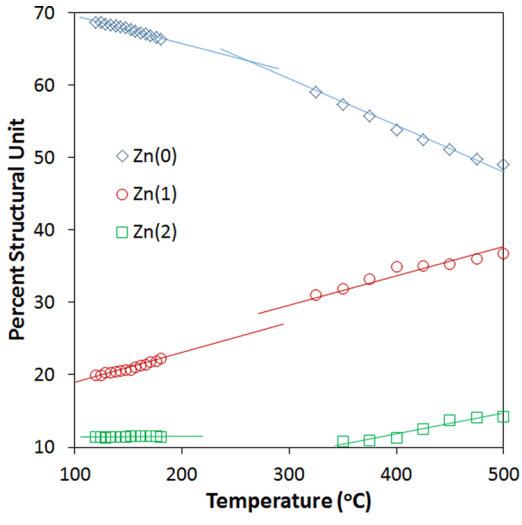

Figure 4. Evolution of the fractions of $Zn^{(0)}$, $Zn^{(1)}$, and $Zn^{(2)}$ structural units measured by Raman spectroscopy as a function of temperature.

DOI: 10.1021/acs.jpcb.7b10857
J. Phys. Chem. B 2017, 121, 11210−11218

Table 1. Comparison of the Relative Fractions of $Zn^{(0)}$, $Zn^{(1)}$, and $Zn^{(2)}$ Derived by Raman, AIMD, and ND Measurements (from Zeidler et al.[23]) as a Function of Temperature

	AIMD			ND			Raman		
temperature (K)	$Zn^{(0)}$ (%)	$Zn^{(1)}$ (%)	$Zn^{(2)}$ (%)	$Zn^{(0)}$ (%)	$Zn^{(1)}$ (%)	$Zn^{(2)}$ (%)	$Zn^{(0)}$ (%)	$Zn^{(1)}$ (%)	$Zn^{(2)}$ (%)
600	60	34	6	60	30	10	59	32	9
700				49	31	20	52	35	13
800	53	41	6	42	30	28			
900	43	49	8	42	34	24			

populations of $Zn^{(1)}$ and $Zn^{(2)}$ increase with temperature. Hence, the fraction of edge-sharing tetrahedra increases with temperature, as previously suggested.[5,7] This overall trend is consistent with recent neutron diffraction (ND) measurements[23] and our AIMD simulation results. Table 1 compares the relative fractions of structural units obtained by AIMD, ND, and Raman measurements. The three techniques are in qualitative agreement and show a systematic increase in the fraction of edge-sharing tetrahedra with temperature above the melting point. Unfortunately, CPU limitations do not allow AIMD simulations in the low-temperature region, and similarly, ND experiments at low temperature are precluded because of rapid crystallization.

Nevertheless, a comparison between the high- and low-temperature behavior is possible by Raman spectroscopy, and interestingly, the rate of change of the relative populations of structural units appears to be different, as depicted in Figure 4. Whereas the rate of formation of $Zn^{(1)}$ shows minimal variability, the rate of decrease of $Zn^{(0)}$ and the rate of increase of $Zn^{(2)}$ appear to be significantly greater at high temperature. This would imply that the rate of conversion of corner- to edge-sharing tetrahedra is different at high and low temperatures. This is indeed confirmed by plotting the ratio of corner- to edge-sharing tetrahedra defined by eq 1 as a function of temperature.

$$\frac{CS}{ES} = \frac{Zn^{(0)} + \frac{Zn^{(1)}}{2}}{Zn^{(2)} + \frac{Zn^{(1)}}{2}} \quad (1)$$

The logarithm of this ratio is plotted as a function of T_g-scaled inverse temperature in Figure 5. The plot clearly reveals two distinct regimes at high and low temperatures. A van't Hoff analysis of these data yields enthalpy of reaction ΔH = 8.02 kJ/mol at high temperature, whereas it is more than 4 times lower, ΔH = 1.84 kJ/mol, at low temperature. These values are comparable to the enthalpy of formation of edge-sharing tetrahedra previously measured in Ge−Se melts.[30]

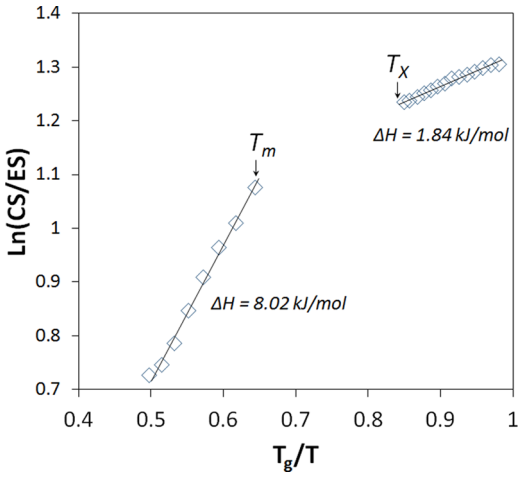

Figure 5. Evolution of the ratio of corner- to edge-sharing tetrahedra as a function of temperature. The temperature is normalized by T_g for easy comparison with a fragility plot.

The spectroscopic data of Figure 5 clearly indicate that the temperature dependence of the melt structure follows two different trends at high and low temperatures. It remains to determine how this structural evolution affects the transport properties of the liquid and its temperature dependence, that is, the fragility.

3.2. Correlation between the Fraction of Structural Motifs and Fragility. A correlation between fragility and the population of edge-sharing motifs in tetrahedral liquids has been previously suggested by molecular dynamic.[17] In particular, it was shown that for systems of intermediate fragility, such as $ZnCl_2$ and $GeSe_2$, increasing the number of edge-sharing motifs by tuning the anion polarizability leads to a concomitant increase in fragility.

This correlation can be qualitatively illustrated by invoking the contribution of corner- and edge-sharing motifs to the structural dimensionality. Figure 6 depicts the two extreme cases of tetrahedral liquids composed purely of corner-sharing and edge-sharing tetrahedra. The corner-sharing liquid (Figure 6a) exhibits a three-dimensional structure reminiscent of the archetypically strong liquid SiO_2, whereas the edge-sharing liquid (Figure 6b) exhibits a one-dimensional structure reminiscent of the fragile selenium melt. A correlation between structural dimensionality and fragility has also been previously observed in the covalent network system As−Se.[31]

This qualitative correlation can be quantified more systematically using the constraint counting formalism and its relation to configurational entropy.[32−34] Topological principles of network systems surmise that three-dimensional atomic motions are restricted by restoring forces imposed by bond-stretching and angular constraints.[35,36] The network's ability to deform at no energy cost is then related to the number f = degrees of freedom − constraints on each atom. In that formalism, highly coordinated networks are overconstrained and rigid ($f < 0$), whereas low coordination networks are underconstrained and floppy ($f > 0$).[35]

In turn, it was shown that the f number relates to the configurational entropy, S_c, of the system according to

$$S_c = fNk \ln \Omega \quad (2)$$

where Ω is the number of accessible microstates per atomic degree of freedom (independent of f), k is the Boltzmann constant, and N is the number of atoms.[32,33] Hence, any structural motif that lowers the number of constraints would increase f and S_c and in turn lower the viscosity, η, according to the Adam−Gibbs equation,[37] where η_o is the viscosity and B is a fitting parameter

DOI: 10.1021/acs.jpcb.7b10857
J. Phys. Chem. B 2017, 121, 11210−11218

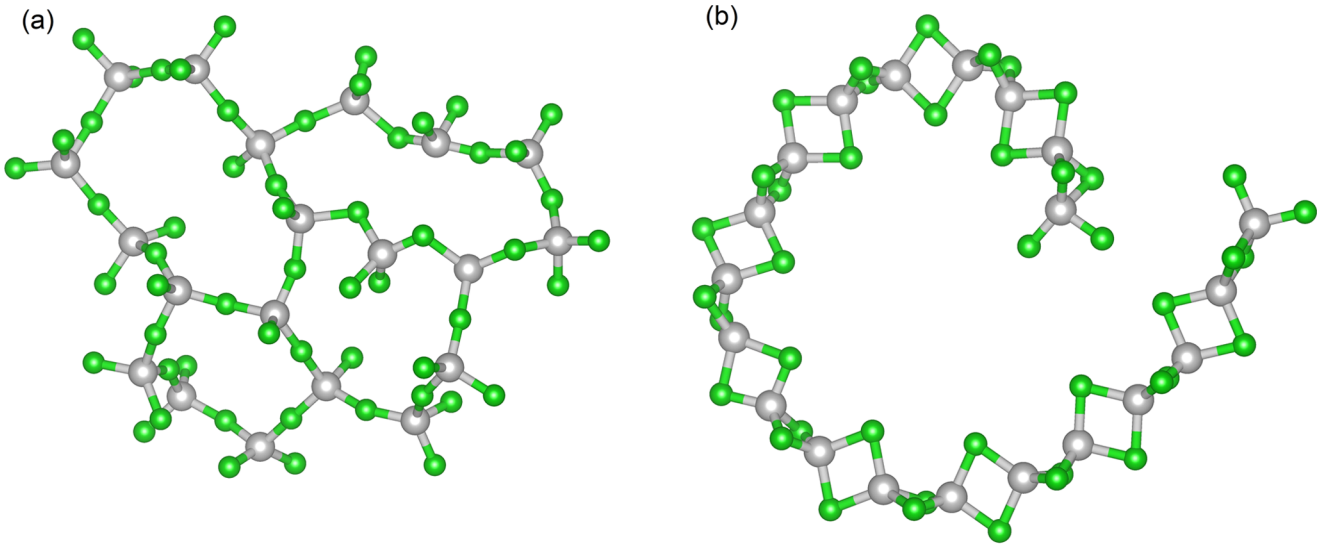

Figure 6. Structure of tetrahedral liquids composed of (a) corner-sharing motifs only and (b) edge-sharing motifs only.

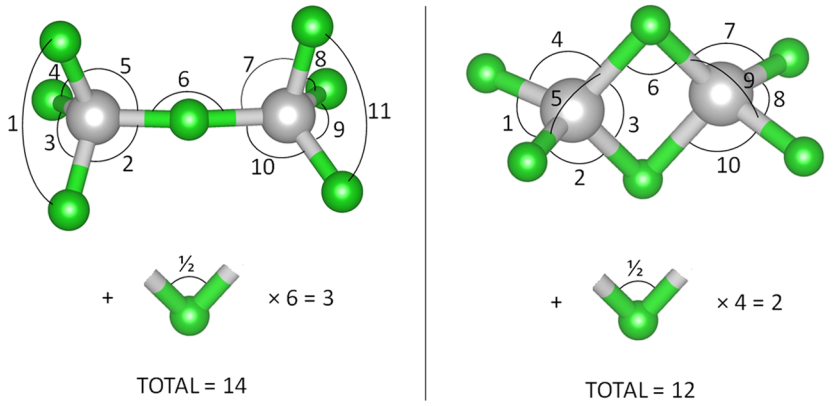

Figure 7. Angular constraint counting for a pair of corner- and edge-sharing tetrahedra. Each outer bridging Cl is assigned a half angular constraint.

$$\log \eta = \log \eta_o + \frac{B}{TS_c} \tag{3}$$

It can in fact be shown that the conversion from corner- to edge-sharing tetrahedra serves precisely that function. Indeed, whereas the number of bond-stretching constraints is the same between the two motifs, the number of angular constraints is actually lower in the edge-sharing unit. As depicted in Figure 7, only two constraints are sufficient to define the angles of the four-member ring in the edge-sharing unit and only four outer chlorine atoms remain, each contributing a half constraint, in comparison to six outer atoms for the corner-sharing unit. This leads to a total of 14 angular constraints for the corner-sharing pair, as opposed to 12 for the edge-sharing pair. Hence, an increase in the edge-sharing tetrahedra population will effectively lower f, S_c, and viscosity η.

But most interestingly, it is the rate of conversion between the two motifs that governs the fragility, as can be derived from eq 3. For example, a rapid change in S_c with temperature would lead to a pronounced non-Arrhenius viscosity−temperature dependence characteristic of fragile systems. Hence, the notable difference in the conversion rate revealed in Figure 5 (and the concomitant variation in S_c) would be indicative of a fragile-to-strong transition in $ZnCl_2$ melts. The slow change in S_c near T_g would indicate a strong behavior at low temperature, whereas the faster change in S_c above T_m would indicate a fragile behavior at high temperature. It remains to be determined whether the structural behavior depicted in Figure 5 correlates with transport properties measured experimentally in the same temperature ranges.

3.3. Viscosity−Temperature Dependence of $ZnCl_2$ Melts. Several sets of experimental viscosity data for $ZnCl_2$ are available and are in excellent agreement with each other, as depicted in Figure 8[11−14] However, because of the excessively hygroscopic nature of $ZnCl_2$, no direct viscosity measurements have ever been performed near the glass-transition temperature, T_g, and the fragility assignment therefore only relies on viscosity values measured at high temperature above the melting point. A fit of these viscosity data using the MYEGA equation[34] yields a fragility index m = 59, as shown is Figure 8.

Although no viscosity values are available at low temperature, it is still possible to estimate the fragility index near T_g calorimetrically using the following equation[39−42]

$$m = \frac{E_a}{RT_g \ln 10} \tag{4}$$

where E_a is the activation energy and T_g is the standard glass-transition temperature measured at 20 K/min. As shown by Moynihan et al.,[43,44] the activation energy, E_a, can be estimated calorimetrically using the scan rate method depicted in Figure

DOI: 10.1021/acs.jpcb.7b10857
J. Phys. Chem. B 2017, 121, 11210−11218

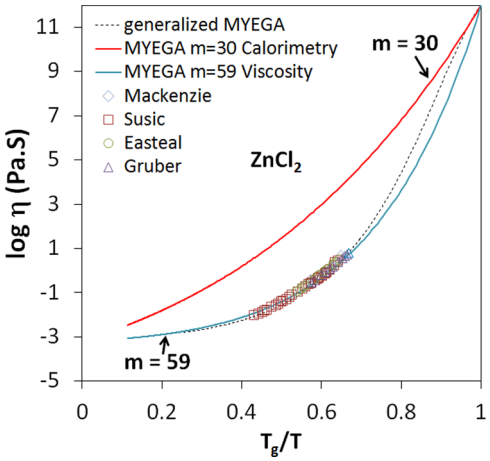

Figure 8. Fragility plot for $ZnCl_2$. The blue line is a fit to the data of Easteal,[11] Gruber,[12] Šušic,[13] and Mackenzie[14] using the MYEGA equation,[34] yielding fragility index $m = 59$. The red line is the viscosity predicted by the MYEGA equation using fragility index $m = 30$ determined by calorimetry neat T_g. The dotted line is a fit using the generalized MYEGA equation.[38]

9. In this method, the system is cooled and reheated at the same rate ($Q_c = Q_h$) across the glass transition and the process is repeated for a series of increasing rates, as shown in Figure 9a. The slope of $\ln(Q)$ versus $1/T_g$ is equal to E_a/R, and a linear fit yields $E_a = 2.21 \times 10^2$ kJ/mol, as shown in Figure 9b. The resulting value of the fragility index near T_g is then $m = 30$. This value is about 2 times smaller than the high-temperature value, thereby confirming the existence of a fragile-to-strong transition in $ZnCl_2$ melts, in qualitative accord with the spectroscopic results of Figure 5. The corresponding viscosity−temperature dependence is plotted in Figure 8 using the MYEGA equation with $m = 30$. The fragile-to-strong transition is modeled using the generalized MYEGA equation[38] (dotted line). The fragile-to-strong transition factor for $ZnCl_2$ is $F = m'/m \approx 2$ (where m' is the high-temperature fragility). This value of F is lower than that found for metallic glasses ($F \approx 3-8$)[38] but comparable to that recently found in covalent phase-change material systems.[45]

Overall, these results provide a structural origin for the fragile-to-strong transition in tetrahedral liquid $ZnCl_2$. Indeed, the fragile-to-strong transition correlates with the kinetic of formation of edge-sharing tetrahedra in the melt. Moreover, this correlation is expected from constraint counting principles and is consistent with molecular dynamics calculations.[17] This raises the question of whether this type of transition is common to other tetrahedral liquids that may form edge-sharing tetrahedra.

3.4. Fragile-to-Strong Transition in $GeSe_2$ Melts. $GeSe_2$ is also a tetrahedral system that, unlike silica, possesses a large fraction of edge-sharing tetrahedra.[46] It is therefore isostructural to $ZnCl_2$ (except for the presence of some homopolar bonds), and the two systems have often been contrasted in previous studies.[5,16,17] In addition, it was reported that the fraction of edge-sharing tetrahedra increases with temperature in supercooled Ge−Se melts in a way similar to that in $ZnCl_2$ and with a comparable enthalpy of formation, $\Delta H = 5$ kJ/mol.[30] The similarity in behavior may therefore extend to the presence of an analogous fragile-to-strong transition in $GeSe_2$. Indeed, such a transition was postulated by Grande et al.,[47] and a fragile-to-strong transition was recently shown in the close-by system $Ge_{30}Se_{70}$.[48] In fact, high-temperature viscosity data[49,50] for $GeSe_2$ plotted in Figure 10 show an abnormal trend that would be consistent with the onset of a fragile-to-strong transition. However, no viscosity data are available at low temperature that could confirm that trend, due to the tendency for rapid crystallization of $GeSe_2$.

Nevertheless, in the same way as for $ZnCl_2$, the fragility index near T_g can be measured calorimetrically. The results shown in Figure 11 yield fragility index $m = 42$ at low temperature compared with index $m = 105$ obtained by fitting the high-temperature data of Ruska et al.[49] with the MYEGA equation. This result therefore strongly supports the existence of a fragile-to-strong transition in $GeSe_2$, which is reminiscent of the case of liquid $Ge_{15}Te_{85}$.[41] The fragile-to-strong transition is modeled using the generalized MYEGA equation[38] (dotted line). Further viscosity data[49,50] indicate that similar fragile-to-strong

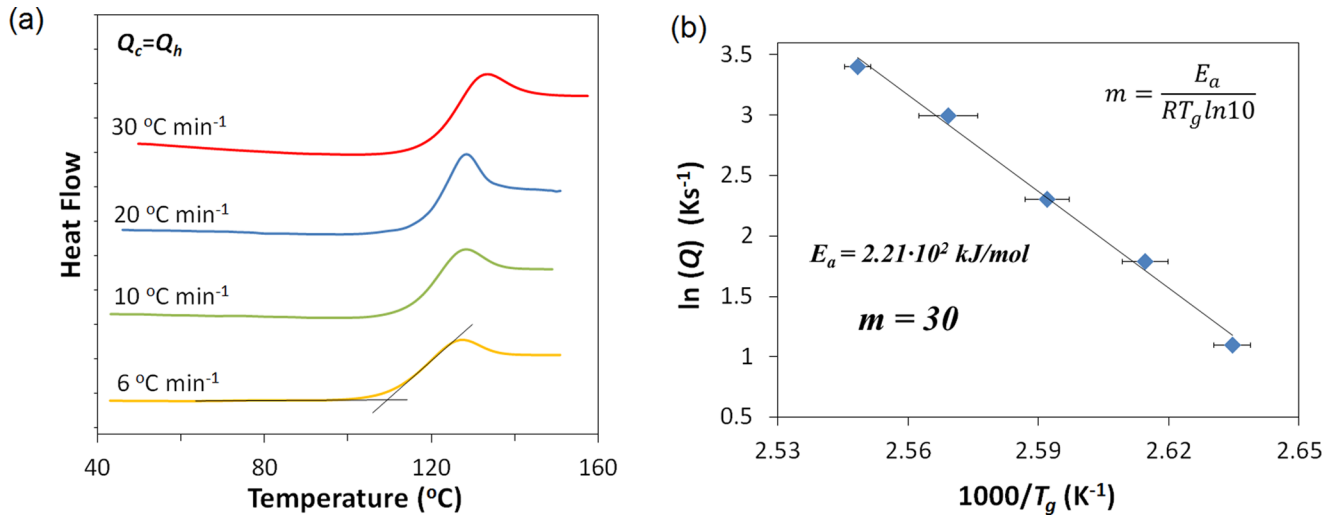

Figure 9. Calorimetric determination of the fragility of $ZnCl_2$ near T_g using Moynihan's scan rate method.[43,44] (a) DSC scan of the glass transition measured at various heating rates after cooling at the same rate. The curves are vertically shifted for clarity. (b) Plot of the natural logarithm of the heating rate against inverse T_g used to determine activation energy for enthalpy relaxation E_a and fragility index m.

DOI: 10.1021/acs.jpcb.7b10857
J. Phys. Chem. B 2017, 121, 11210−11218

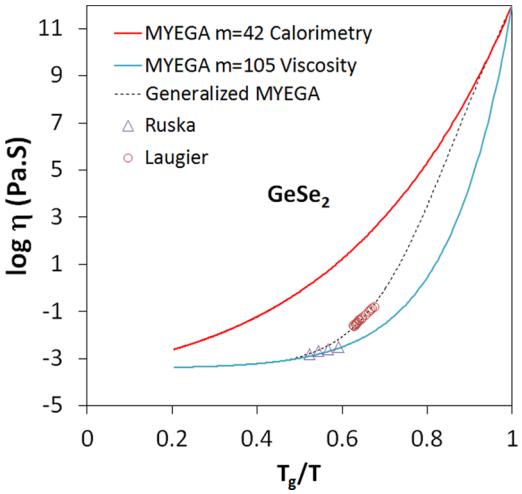

Figure 10. Fragility plot for $GeSe_2$. The blue line is a fit to the data of Ruska[49] using the MYEGA equation yielding fragility index m = 105. The red line is the viscosity predicted by the MYEGA equation using fragility index m = 42 determined by calorimetry near T_g. The dotted line is a fit using the generalized MYEGA equation.[38]

transitions are present in $GeSe_3$ and $GeSe_4$, as will be discussed in a future study.

Although further Raman data on $GeSe_2$ melts are required to unambiguously correlate the fragile-to-strong transition to the rate of formation of edge-sharing tetrahedra, the sum of information available on the Ge−Se system strongly suggests that it is likely the case.

Overall, this emphasizes the rich and peculiar behavior of tetrahedral liquids. Indeed, it has been shown that fragile-to-strong transitions exist in multiple other tetrahedral systems ranging from water[51] and SiO_2[52] to BeF_2.[5353] However, little is known of their structural origin.

4. CONCLUSIONS

Viscosity and calorimetric data indicate that the tetrahedral $ZnCl_2$ melt undergoes a transition from a strong liquid, m = 30, near T_g to a fragile liquid, m = 59, above T_m. Raman spectroscopy data show that this transition is concomitant with a change in the rate of conversion between corner- and edge-sharing tetrahedra in the melt structure with increasing temperature. This is consistent with the prediction from the constraint counting formalism. The latter shows that the formation of edge-sharing tetrahedra increases the configurational entropy and in turn decreases the viscosity. This is also consistent with structural dimensionality considerations, where the increase in the fraction of edge-shared tetrahedral units reduces the dimensionality. Finally, this is consistent with molecular dynamic simulations that show a correlation between fragility and edge-shared tetrahedra. A similar fragile-to-strong transition is found in the isostructural $GeSe_2$, which is also known to exhibit a large fraction of edge-sharing motifs and an increased number of these motifs with temperature. The similarity between the two systems suggests that this type of structural change and their related fragile-to-strong transition may be a common feature of tetrahedral melt.

AUTHOR INFORMATION

Corresponding Author

*E-mail: pierre@u.arizona.edu. Tel: 1-520-322-2311.

ORCID

Pierre Lucas: 0000-0003-1011-0855

Present Addresses

§Institute of Physics, RWTH Aachen University, Aachen 52062, Germany (S.W.).

‖Department of Mechanical Engineering, King Fahd University of Petroleum & Minerals (KFUPM), Dhahran 31261, Kingdom of Saudi Arabia (A.Q.A.).

Notes

The authors declare no competing financial interest.

ACKNOWLEDGMENTS

This project was supported by DOE-MURI grant# DE-EE0005942 under the U.S. DoE Sunshot program. A.Q.A. acknowledges King Fahad University of Petroleum and Minerals (KFUPM) for financial support during his Ph.D. S.W. acknowledges financial support from an Alexander von Humboldt Foundation Feodor Lynen Postdoctoral Research Fellowship.

REFERENCES

(1) Vignarooban, K.; Xu, X.; Wang, K.; Molina, E. E.; Li, P.; Gervasio, D.; Kannan, A. M. Vapor pressure and corrosivity of ternary metal-chloride molten-salt based heat transfer fluids for use in concentrating solar power systems. *Appl. Energy* **2015**, *159*, 206−213.

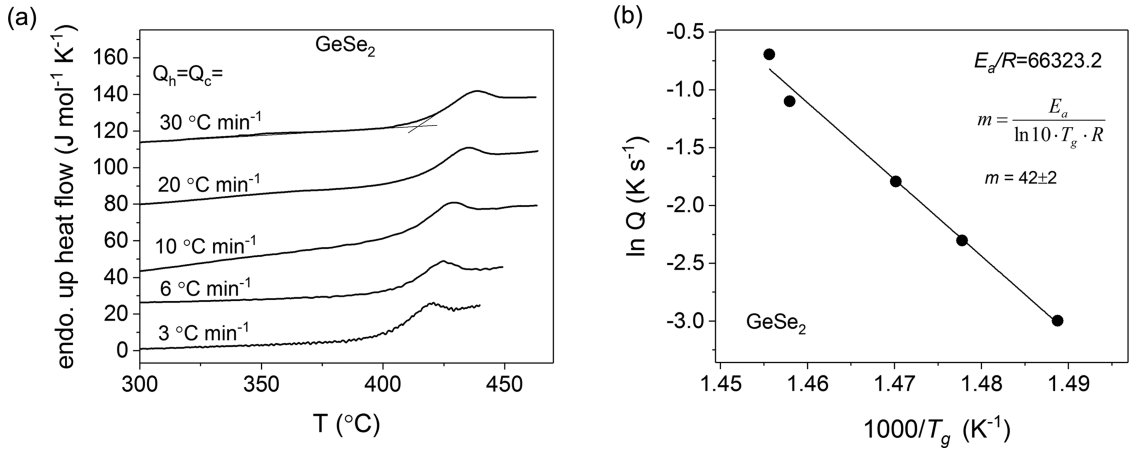

Figure 11. Calorimetric determination of the fragility of $GeSe_2$ near T_g.

DOI: 10.1021/acs.jpcb.7b10857
J. Phys. Chem. B 2017, 121, 11210−11218

(2) Li, P.; Molina, E.; Wang, K.; Xu, X.; Dehghani, G.; Kohli, A.; Hao, Q.; Kassaee, M. H.; Jeter, S. M.; Teja, A. S. Thermal and transport properties of NaCl-KCl-$ZnCl_2$ eutectic salts for new generation high-temperature heat-transfer fluids. *J. Sol. Energy Eng.* **2016**, *138*, No. 054501.
(3) Manga, V. R.; Swinteck, N.; Bringuier, S.; Lucas, P.; Deymier, P.; Muralidharan, K. Interplay between structure and transport properties of molten salt mixtures of $ZnCl_2$−NaCl−KCl: A molecular dynamics study. *J. Chem. Phys.* **2016**, *144*, No. 094501.
(4) Angell, C. A.; Wong, J. Structure and glass transition thermodynamics of liquid zinc chloride from far-infrared, Raman, and probe ion electronic and vibrational spectra. *J. Chem. Phys.* **1970**, *53*, 2053−2066.
(5) Zeidler, A.; Salmon, P. S.; Martin, R. A.; Usuki, T.; Mason, P. E.; Cuello, G. J.; Kohara, S.; Fischer, H. E. Structure of liquid and glassy $ZnCl_2$. *Phys. Rev. B* **2010**, *82*, No. 104208.
(6) Alsayoud, A. Q.; Venkateswara Rao, M.; Edwards, A. N.; Deymier, P. A.; Muralidharan, K.; Potter, B. G.; Runge, K.; Lucas, P. Structure of $ZnCl_2$ melt. Part I: Raman spectroscopy analysis driven by ab initio methods. *J. Phys. Chem. B* **2016**, *120*, 4174−4181.
(7) Yannopoulos, S. N.; Kalampounias, A. G.; Chrissanthopoulos, A.; Papatheodorou, G. N. Temperature induced changes on the structure and the dynamics of the "tetrahedral" glasses and melts of $ZnCl_2$ and $ZnBr_2$. *J. Chem. Phys.* **2003**, *118*, 3197−3214.
(8) Salmon, P. S.; Martin, R. A.; Mason, P. E.; Cuello, G. J. Topological versus chemical ordering in network glasses at intermediate and extended length scales. *Nature* **2005**, *435*, 75−78.
(9) Aliotta, F.; Maisano, G.; Migliardo, P.; Vasi, C.; Wanderlingh, F.; Smith, G. P.; Triolo, R. Vibrational dynamics of glassy and molten zinc chloride. *J. Chem. Phys.* **1981**, *75*, 613−618.
(10) Irish, D. E.; Young, T. F. Raman spectrum of molten zinc chloride. *J. Chem. Phys.* **1965**, *43*, 1765−1768.
(11) Easteal, A. J.; Angell, C. A. Viscosity of molten $ZnCl_2$ and supercritical behavior in its binary solutions. *J. Chem. Phys.* **1972**, *56*, 4231−4233.
(12) Gruber, G. J.; Litovitz, T. A. Shear and structural relaxation in molten zinc chloride. *J. Chem. Phys.* **1964**, *40*, 13−26.
(13) Šušic, M. V.; Mentus, S. V. Viscosity and structure of molten zinc chloride and zinc bromide. *J. Chem. Phys.* **1975**, *62*, 744.
(14) Mackenzie, J. D.; Murphy, W. K. Structure of glass-forming halides. II. Liquid zinc chloride. *J. Chem. Phys.* **1960**, *33*, 366−369.
(15) Wilson, M.; Madden, P. A. Voids, layers, and the first sharp diffraction peak in $ZnCl_2$. *Phys. Rev. Lett.* **1998**, *80*, 532−535.
(16) Sharma, B. K.; Wilson, M. Intermediate-range order in molten network-forming systems. *Phys. Rev. B* **2006**, *73*, No. 060201.
(17) Wilson, M.; Salmon, P. S. Network topology and the fragility of tetrahedral glass-forming liquids. *Phys. Rev. Lett.* **2009**, *103*, No. 157801.
(18) Woodcock, L. V.; Angell, C. A.; Cheeseman, P. Molecular dynamics studies of the vitreous state: Simple ionic systems and silica. *J. Chem. Phys.* **1976**, *65*, 1565−1577.
(19) Kumta, P. N.; Deymier, P. A.; Risbud, S. H. Improved rigid ion model of molten zinc chloride. *Phys. B* **1988**, *153*, 85−92.
(20) Gardner, P. J.; Heyes, D. M. Molecular dynamics computer simulations of molten zinc chloride. *Physica B+C* **1985**, *131*, 227−233.
(21) Angell, C. A.; Rao, K. J. Configurational excitations in condensed matter, and the bond lattice model for the liquid-glass transition. *J. Chem. Phys.* **1972**, *57*, 470−481.
(22) Angell, C. A. Relaxation in liquids, polymers and plastic crystals - strong/fragile patterns and problems. *J. Non-Cryst. Solids* **1991**, *131*−*133*, 13−31.
(23) Zeidler, A.; Chirawatkul, P.; Salmon, P. S.; Usuki, T.; Kohara, S.; Fischer, H. E.; Howells, W. S. Structure of the network glass-former $ZnCl_2$: From the boiling point to the glass. *J. Non-Cryst. Solids* **2015**, *407*, 235−245.
(24) Kresse, G.; Furthmueller, J. Efficient iterative schemes for ab initio total-energy calculations using a plane-wave basis set. *Phys. Rev. B* **1996**, *54*, 11169−11186.
(25) Kresse, G.; Hafner, J. Ab initio molecular dynamics of liquid metals. *Phys. Rev. B* **1993**, *47*, 558−561.
(26) Blöchl, P. E. Projector augmented-wave method. *Phys. Rev. B* **1994**, *50*, 17953−17979.
(27) Kresse, G.; Joubert, D. From ultrasoft pseudopotentials to the projector augmented-wave method. *Phys. Rev. B* **1999**, *59*, 1758−1775.
(28) Perdew, J. P.; Burke, K.; Ernzerhof, M. Generalized gradient approximation made simple. *Phys. Rev. Lett.* **1996**, *77*, 3865−3868.
(29) Le Roux, S.; Jund, P. Ring statistics analysis of topological networks: New approach and application to amorphous GeS_2 and SiO_2 systems. *Comput. Mater. Sci.* **2010**, *49*, 70−83.
(30) Edwards, T. G.; Sen, S. Structure and relaxation in germanium selenide glasses and supercooled liquids: a Raman spectroscopic Study. *J. Phys. Chem. B* **2011**, *115*, 4307−4314.
(31) Yang, G.; Gulbiten, O.; Gueguen, Y.; Bureau, B.; Sangleboeuf, J.-C.; Roiland, C.; King, E. A.; Lucas, P. Fragile-strong behavior in the As_xSe_{1-x} glass forming system in relation to structural dimensionality. *Phys. Rev. B* **2012**, *85*, No. 144107.
(32) Gupta, P. K.; Mauro, J. C. Composition dependence of glass transition temperature and fragility. I. A topological model incorporating temperature-dependent constraints. *J. Chem. Phys.* **2009**, *130*, No. 094503.
(33) Naumis, G. G. Energy landscape and rigidity. *Phys. Rev. E* **2005**, *71*, No. 026114.
(34) Mauro, J. C.; Yue, Y.; Ellison, A. J.; Gupta, P. K.; Allan, D. C. Viscosity of glass-forming liquids. *Proc. Natl. Acad. Sci. U.S.A.* **2009**, *106*, 19780−19784.
(35) Thorpe, M. F. Continuous deformations in random networks. *J. Non-Cryst. Solids* **1983**, *57*, 355−370.
(36) He, H.; Thorpe, M. F. Elastic properties of glasses. *Phys. Rev. Lett.* **1985**, *54*, 2107−2110.
(37) Ediger, M. D.; Angell, C. A.; Nagel, S. R. Supercooled Liquids and Glasses. *J. Phys. Chem.* **1996**, *100*, 13200−13212.
(38) Zhang, C.; Hu, L.; Yue, Y.; Mauro, J. C. Fragile-to-strong transition in metallic glass-forming liquids. *J. Chem. Phys.* **2010**, *133*, No. 014508.
(39) Crowley, K. J.; Zografi, G. The use of thermal methods for predicting glass-former fragility. *Thermochim. Acta* **2001**, *380*, 79−93.
(40) Wang, L.-M.; Velikov, V.; Angell, C. A. Direct determination of kinetic fragility indices of glassforming liquids by differential scanning calorimetry: kinetic versus thermodynamic fragilities. *J. Chem. Phys.* **2002**, *117*, 10184−10192.
(41) Wei, S.; Lucas, P.; Angell, C. A. Phase change alloy viscosities down to Tg using Adam-Gibbs-equation fittings to excess entropy data: A fragile-to-strong transition. *J. Appl. Phys.* **2015**, *118*, No. 034903.
(42) Wei, S.; Coleman, G. J.; Lucas, P.; Angell, C. A. Glass transitions, semiconductor-metal transitions, and fragilities in Ge-V-Te (V = As, Sb) liquid alloys: the difference one element can make. *Phys. Rev. Appl.* **2017**, *7*, No. 034035.
(43) Moynihan, C. T.; Lee, S.-K.; Tatsumisago, M.; Minami, T. Estimation of activation energies for structural relaxation and viscous flow from DTA and DSC experiments. *Thermochim. Acta* **1996**, *280*−*281*, 153−162.
(44) Moynihan, C. T.; Easteal, A. J.; Wilder, J.; Tucker, J. Dependence of the glass transition temperature on heating and cooling rate. *J. Phys. Chem.* **1974**, *78*, 2673−2677.
(45) Orava, J.; Weber, H.; Kaban, I.; Greer, A. L. Viscosity of liquid Ag-In-Sb-Te: Evidence of a fragile-to-strong crossover. *J. Chem. Phys.* **2016**, *144*, No. 194503.
(46) Petri, I.; Salmon, P. S.; Fischer, H. E. Defects in a disordered world: the structure of glassy $GeSe_2$. *Phys. Rev. Lett.* **2000**, *84*, 2413−2416.
(47) Stølen, S.; Grande, T.; Johnsen, H.-B. Fragility transition in $GeSe_2$-Se liquids. *Phys. Chem. Chem. Phys.* **2002**, *4*, 3396−3399.
(48) Orava, J.; Hewak, D. W.; Greer, A. L. Fragile-to-strong crossover in supercooled liquid Ag-In-Sb-Te studied by ultrafast calorimetry. *Adv. Funct. Mater.* **2015**, *25*, 4851−4858.

DOI: 10.1021/acs.jpcb.7b10857
J. Phys. Chem. B 2017, 121, 11210−11218

(49) Ruska, J.; Thurn, H. Change of short-range order with temperature and composition in liquid germanium selenide (Ge_xSe_{1-x}) as shown by density measurements. *J. Non-Cryst. Solids* **1976**, *22*, 277−290.
(50) Laugier, A.; Chaussemy, G.; Fornazero, J. Viscosity of the glass-forming germanium-selenium liquid solutions. *J. Non-Cryst. Solids* **1977**, *23*, 419−429.
(51) Ito, K.; Moynihan, C. T.; Angell, C. A. Thermodynamic determination of fragility in liquids and a fragile-to-strong liquid transition in water. *Nature* **1999**, *398*, 492−495.
(52) Saika-Voivod, I.; Poole, P. H.; Sciortino, F. Fragile-to-strong transition and polyamorphism in the energy landscape of liquid silica. *Nature* **2001**, *412*, 514−517.
(53) Hemmati, M.; Moynihan, C. T.; Angell, C. A. Interpretation of the molten BeF_2 viscosity anomaly in terms of a high temperature density maximum, and other waterlike features. *J. Chem. Phys.* **2001**, *115*, 6663−6671.

DOI: 10.1021/acs.jpcb.7b10857
J. Phys. Chem. B 2017, 121, 11210−11218